# An Introduction to Active Matter Models and Properties of Active Systems

Joost de Graaf[1,*]

[1] *Institute for Theoretical Physics, Center for Extreme Matter and Emergent Phenomena, Utrecht University, Princetonplein 5, 3584 CC Utrecht, The Netherlands*

(Dated: March 5, 2026)

FIG. 1. **The Archetypal Active Matter System:** Flocks of the common starling — known as murmurations — can form and change shape swiftly. Murmurations form over the birds' communal roosting site, close to dusk, and are believed help to ward off predators by producing mesmerizing patterns. Copyright on Image: Owen Humpreys / PA Wire.

## I. INTRODUCTION

In a previous lecture, we have examined systems that were out-of-equilibrium, but in a sense close to equilibrium. Recall that in deriving *Dynamic Density Functional Theory* from the *Smoluchowski equation* following Ref. [1], we observed that the return to equilibrium is governed by measuring the distance to equilibrium in terms of the potential and probability density — equilibrium was defined by the Boltzmann distribution. Ultimately, this led to a linear response theory for the evolution of the particle density in terms of the gradient of the (local) chemical potential.

Here, we will turn our attention to systems that are intrinsically far away from equilibrium. Active matter is a term that describes a class of systems, in which energy is constantly consumed to perform work, and broadly can be found in all the known phases: gas, liquid, fluid, solid, and several (presumably all) liquid-crystalline mesophases. These systems defy description using the standard framework of statistical mechanics, due to their strong departure from equilibrium, despite having apparent similarities to their passive counterparts.

Activity is the norm in biology. On our length scale, we encounter flocks of birds [2] (see Fig. 1), schools of fish [3], and, of course, human crowds [4–6]; on the mesoscopic level examples are found

* j.degraaf@uu.nl

in dividing and moving bacteria [7–9], sperm [10–12], and algae [13, 14]; and on the nanoscopic level, transport along the cytoskeleton is achieved by myosin motors [15].

Recent years have seen a huge increase in studies into systems consisting of self-propelled particles, in particular artificial ones in the colloidal regime [16–29]. These self-propelled colloids show promise as physical model systems for complex biological behavior (bacteria moving collectively) and could be used to answer fundamental questions concerning out-of-equilibrium statistical physics [30, 31]. From the perspective of physical chemistry, much remains poorly understood about the way many of these artificial swimmers move [19, 32–38] and form collective states. This makes the field of active matter fruitful for experimental study and provides ample opportunity for interaction with theory.

The above exemplifies the range of length and time scales, which the field of active matter encompasses, as well as its diversity. Physical features of interest in these systems are the apparent ability to 'phase separate' at much lower density than in equilibrium. This is known as *Motility Induced Phase Separation* (MIPS) in an *Active Brownian Particle* (ABP) system. We will cover this model in greater detail in these notes. Another form of *non-equilibrium* phase transition is found in the *Vicsek model*, which was derived by Tamás Vicsek and collaborators in 1995 [39]. We will also cover this model and its main features. From this model a hydrodynamic theory can be derived that describes the long-time and large-scale dynamics, often referred to as the *Toner-Tu* model [40–42]. We will not cover this derivation here in the interest of time and because it requires more detailed knowledge of hydrodynamic theory.

Lastly, simulations play an important role in the study of active matter, as the parameters are more readily tuned and the results 'cleaner' than can be obtained in experiment. Additionally, these numerical simulations inform the development of theories that are applicable far from equilibrium. In many active systems there is also a strong connection to topology and the motion of defects [43–47], which unfortunately falls outside the scope of these notes. The interplay between dynamics, geometry, defects, and topology is of primary interest to understand structure in biology and the manufacture of new metamaterials. We refer the interested reader to Refs. [48, 49] for further information. At the end of this set of notes, we hope to convince you that active matter has become a rich and dynamic field in the roughly 30 years since its inception.

## II. BEHAVIOR OF A SINGLE ACTIVE PARTICLE

In the following, we will consider active systems comprising self-propelled particles[1]. Among many other aspects, these behave differently from passive ones when it comes to their diffusivity. A single active particle of a certain size violates the Stokes-Einstein relation [50], which states that the translational diffusion coefficient (of a sphere) is given by

$$D_t = \frac{k_\mathrm{B}T}{6\pi\eta a}, \tag{1}$$

where $k_\mathrm{B}$ is Boltzmann's constant, $T$ the temperature, $\eta$ is the viscosity, and $a$ is the radius. If the self-propelled particle does not experience Brownian motion, it would move with a constant speed along a straight line. This means that its mean-squared displacement (MSD) is ballistic. Rotational reorientation due to Brownian collisions with the fluid cause this self-propulsion-induced ballistic regime to transition into a diffusive regime, on a time governed by the rotational diffusion. Thus, when compared to its passive equivalent, a new ballistic regime emerges at intermediate times and the diffusivity is enhanced as a consequence.

[1] The terms active particles and self-propelled particles are used interchangeably throughout these lecture notes, though technically active particles belong to a more general class. Division, fluid pumping, and performing chemical reactions are examples of active processes that do not (necessarily) involve self-propulsion.

### A. Enhanced Diffusion for Self-Propelled Colloids

Let us make this explicit by writing down the appropriate equations of motion in two dimensions[2] (2D) [22]. The self-propelled particle is assumed to be colloidal in size and its speed $v_0$ is sufficiently small for the dynamics to be overdamped. Then, the equations of motion are given by

$$\dot{\boldsymbol{r}}(t) = v_0\hat{\boldsymbol{n}}(t) + \sqrt{2D_t}\boldsymbol{\xi}_t(t); \tag{2}$$

$$\dot{\theta}(t) = \sqrt{2D_r}\xi_r(t) \tag{3}$$

where $\boldsymbol{r}(t)$ denotes the active colloid's position coordinate and the 'dot' indicates a time derivative. The direction of self-propulsion is given by the unit vector $\hat{\boldsymbol{n}} = (\cos\theta, \sin\theta)$, where $\theta(t)$ is the angle with respect to the $x$-axis (or another axis, the choice is irrelevant). The $\xi$ are stochastic variables and these noise terms satisfy $\langle\boldsymbol{\xi}_t(t)\rangle = \boldsymbol{0}$, $\langle\xi_r(t)\rangle = 0$, $\langle\boldsymbol{\xi}_t(t)\otimes\boldsymbol{\xi}_t(t')\rangle = \mathbb{I}_2\delta(t-t')$, and $\langle\xi_r(t)\xi_r(t')\rangle = \delta(t-t')$. Here, $\delta$ is the Dirac delta function (distribution), $\otimes$ the Kronecker product, and $\mathbb{I}_2$ the $2\times 2$ identity matrix.

The physical assumption underlying Eqs. (2) and (3) is that the self-propelled particle is a regular Brownian particle, its self-propulsion is directed along the plane, and its direction of self-propulsion changes through a diffusion process. The common assumption is that the following diffusion coefficient

$$D_r = \frac{k_\mathrm{B}T}{8\pi\eta a^3}, \tag{4}$$

holds for the reorientation. However, this assumes free three-dimensional (3D) Brownian reorientation, which might not be applicable for every experimental system [34, 38].

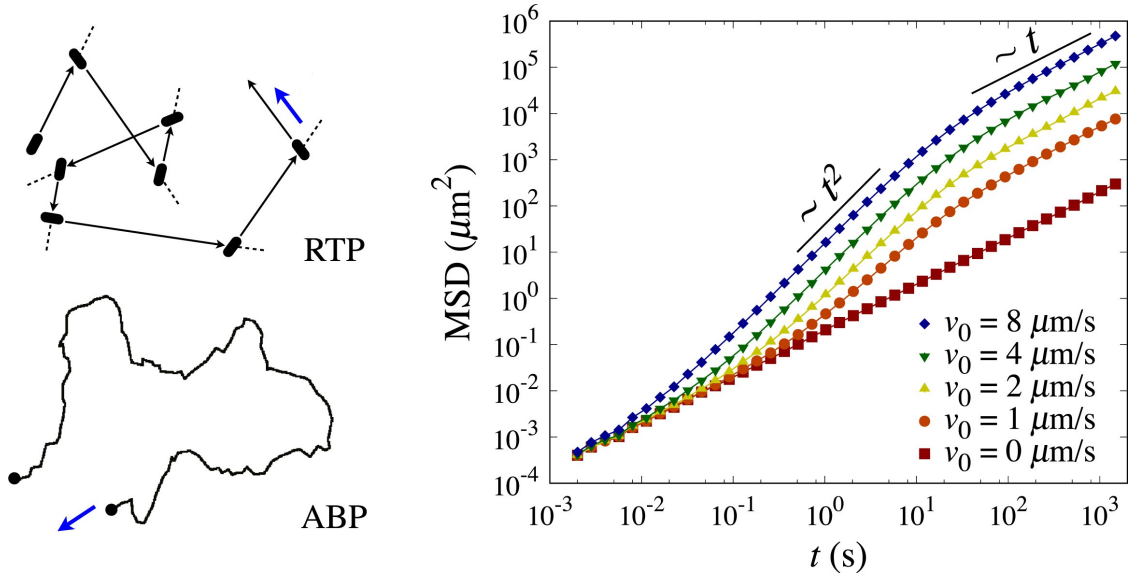


FIG. 2. **Active Brownian and Run-and-Tumble Particles:** On the left two types of active particle reorientation dynamics are shown. (top) Run-and-tumble particles (RTPs) change their direction stochastically by a mean angle. (bottom) Active Brownian particles (ABPs) reorient via rotational diffusion. In both cases the blue arrow indicates the direction of travel. The right shows mean-squared displacements (MSDs) for active particles. These have a long-time enhanced diffusion regime, intermediate-time ballistic motion, and plain diffusive motion at very short times. The figure is adapted from Ref. [54].

[2] The assumption of 2D motion is reasonable for most active particles, as their hydrodynamic dipole nature and self-propulsion tends to concentrate them close to walls. In fact, this tendency to be close to surfaces can be exploited to guide active particles using obstacles [34, 51–53]. An additional assumption needs to be made, namely that the active particle's direction of propulsion is in-plane. This turns out to be experimentally reasonable [22, 34, 53], but is not yet fully understood theoretically. The statement "this is not understood" applies to features of active matter, which offers opportunities and challenges, but is also somewhat unfortunate given the age of the field.

Note that Eq. (3) can be solved separately from Eq. (2), which gives a route toward determining properties of the system. Clearly, both are stochastic differential equations, we therefore should examine properties of the mean (zero) and higher order moments (variance, *etc.*). Analysis of the equations of motion shows that the mean-squared displacement (MSD) is given by

$$\langle |\boldsymbol{r}(t)|^2 \rangle = 4D_t t + 2v_0^2 \tau_r^2 \left[ \frac{t}{\tau_r} + \exp\left( -\frac{t}{\tau_r} \right) - 1 \right], \tag{5}$$

where $\tau_r = 1/D_r$ is the rotational Brownian time. This MSD trend is visualized in Fig. 2.

**Exercise 1:** Here, you will show that Eq. (5) holds.

(a) Perform the first steps in computing the MSD. You should arrive at an expression that contains $\langle \hat{\boldsymbol{n}}(t) \cdot \hat{\boldsymbol{n}}(t') \rangle$.

(b) What do you expect to find for the behavior of this orientational correlation with time on physical grounds?

(c) Show that $\langle \hat{\boldsymbol{n}}(t) \cdot \hat{\boldsymbol{n}}(t') \rangle = \langle \cos(\theta(t) - \theta(t')) \rangle$. How do you expect the difference to be distributed? Argue that you can instead compute $\langle \cos \Delta\theta(t - t') \rangle$, where you define $\Delta\theta$ to be the angle difference. Why is this dependent on the time difference only? Provide the expression for $\langle \Delta\theta(t)^2 \rangle$. What does this represent physically?

(d) Compute the desired average by considering the expectation value of $\cos(aX)$ with $X$ a Gaussian random variable that has mean $\mu$ and variance $\sigma^2$ and $a$ a prefactor. Use an appropriate Gaussian integral to compute $\langle \exp(iaX) \rangle$ to arrive at an expression for $\langle \cos(aX) \rangle$.

(e) Use your expression from (d) to complete the calculation of $\langle \cos \theta(t - t') \rangle$ and Eq. (5).

(f) Use Eq. (5) to demonstrate that for small times ($t \ll \tau_r$) the motion is ballistic

$$\langle |\boldsymbol{r}(t)|^2 \rangle = 4D_t t + v_0^2 t^2, \tag{6}$$

while for long times ($t \gg \tau_r$) the motion is diffusive

$$\langle |\boldsymbol{r}(t)|^2 \rangle = (4D_t + 2v_0^2 \tau_r) t. \tag{7}$$

We should remark that the expression in Eq. (6) is to date the most common form by which experimental measurements are fitted for the active velocity. It has proven itself remarkably robust since it was proposed [22], though here and in subsequent appearances [55] there are small issues with the derivation, also see the supplemental information to Ref. [38].

It might be tempting to assume that a single active particle is now nothing more than a regular Brownian (passive) particle with a slightly higher effective translational diffusion coefficient $D_{\text{eff}} = D_t + v^2 \tau_r / 2$ or equivalently described as a particle at a higher effective 'ambient' temperature. However, this apparent equivalence can lead to problems when one then attempts to apply statistical mechanics to such systems. That is, active systems are well known to phase separate at much lower densities than their Brownian counterparts, and considering Brownian systems at a greater effective temperature would impede rather than produce phase separation.

When considering bacterial systems, the statistics of reorientation will need to be modified. It turns out that biological systems typically have an active means of achieving reorientation, referred

to as *run-and-tumble*, see Fig. 2 for the difference between run-and-tumble particles (RTPs) and ABPs. A flagellated organism such as *E. coli* achieves self-propulsion using a bundle of flagella that is elastohydrodynamically twisted together in a rotating helical shape to achieve motion [56]. Kicking out one of the flagella allows *E. coli* to change its direction, after which it retwists the flagellum into the bundle and continues more or less straight [56]. The statistics of this reorientation was recently accurately characterized [57], but the mechanism or reorientation does not impact significantly the concept of enhanced *translational* diffusion. In a bacterium, this enhancement can be crucial element in nutrient collection and waste management.

### B. Barriers break Equilibrium Physics

In this section, we demonstrate that active systems cannot be mapped onto equilibrium systems. Strikingly, it will turn out to be possible to construct a 'Maxwell demon' of sorts. That is, work may be extracted by coupling a simple system to an *active* bath, which is possible because the system is out of equilibrium. Figure 3 illustrates the process discovered in the group of Roberto Di Leonardo [58, 59], by which a microscopic gear harvests work from a bacterial bath.

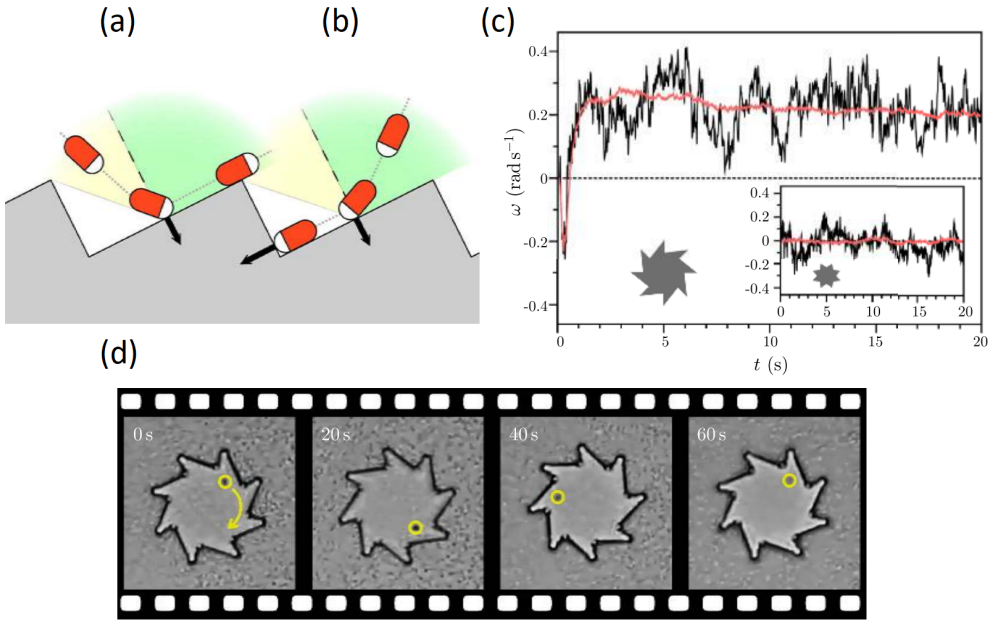


FIG. 3. **Activity enables the Harvesting of Work from using Microgears:** (a,b) Sketch of the collision of a single bacterium with a rectifying boundary: (a) bacteria coming from the left area with respect to the normal, leave the gear, while (b) bacteria coming from the right, get stuck at the corner exerting a torque on the rotor. The arrows represent the forces exerted by the bacteria on the rotor. (c) Angular velocity $\omega$ of the micromotor as a function of time: the black line refers to a single run; the red (lighter) line is the average over 100 independent runs. After a short transient regime (due to the initial configuration of bacteria), a fluctuating velocity around a mean value $\omega_0 \approx 0.21$ rad/s is observed. Inset: The same as the main plot for a micromotor with symmetric teeth, which does not rotate (on average). (d) A nanofabricated asymmetric gear (48 $\mu$m external diameter, 10 $\mu$m thickness) rotates clockwise at 1 rpm when immersed in an active bath of motile *E. coli* cells, visible in the background. The gear is sedimented at a liquid-air interface to reduce friction. The circle points to a black spot on the gear that is used for visual angle tracking. Image composition and caption are adapted from Ref. [55] with reference to the original sources Ref. [58] for (a-c) and Ref. [59] for (d).

The key point to understanding the rotation of a gear is illustrated in Fig. 3a,b. An asymmetric 'ratchet' potential leads to a different interaction with an active particle, depending on the angle of ingress. Here, the active particles are illustrated as spherocylinders. This shape magnifies the ratchet effect due to the torque generated on the particle, when it interacts with a wall. However, the effect is still present for point-like or spherical self-propelled particles [60, 61]. In this case, the rectifying properties of the ratchet are caused by the fact that active particles need to reorient to move out of the corner, either via diffusion or tumbling.

**Exercise 2:** In this exercise, we will consider the rectification of active RTPs by a ratchet potential. This is a system that is equivalent to the gear, with the exception that the ratchet potential is fixed and causes a preferentially rightward current of active particles. A situation that cannot be present in equilibrium (on average).

To simplify the calculation, we consider particles that move in one dimension, say along the $x$-axis, and can tumble between motion directed in the positive and negative direction with free (in the absence of the ratchet potential) speed $v$. Assume that the probability density of right-moving (positive $x$-axis) active particles at position $x$ and time $t$ is given by $R(x,t)$ and equivalently the left-moving population by $L(x,t)$. The particle tumbles with frequency $\alpha$. Hint: You may want to make use of an algebraic manipulation package (*e.g.*, `Mathematica`) to help solve this problem.

(a) Argue why the following expressions hold:

$$\frac{\partial R}{\partial t} = -\frac{\partial}{\partial x}(v_R R) - \frac{\alpha}{2}R + \frac{\alpha}{2}L; \tag{8}$$

$$\frac{\partial L}{\partial t} = \frac{\partial}{\partial x}(v_L L) + \frac{\alpha}{2}R - \frac{\alpha}{2}L, \tag{9}$$

where $v_R$ and $v_L$ are effective velocity values of the motion in the ratchet potential toward the right and left, respectively. They are expected to depend on position, as we will see later.

(b) Consider the total probability density $P = R + L$ and introduce the flux $J = v_R R - v_L L$. Group the terms to obtain a new differential equation

$$\frac{\partial P}{\partial t} = -\frac{\partial}{\partial x}J. \tag{10}$$

(c) Now take the time derivative of Eq. (10). Substitute back into this the identities that you previously derived and set the double time derivative of $P$ to zero. What does this mean physically? Group the terms containing an $\alpha$ to the left-hand side to obtain

$$\frac{\partial J}{\partial t} + \alpha J = v_R\frac{\partial}{\partial x}(v_R R) - v_L\frac{\partial}{\partial x}(v_L L) + \frac{\alpha}{2}(v_R - v_L)P. \tag{11}$$

Assume steady state, which *via* Eq. (10) implies that $J$ is a constant in time. This is reasonable!

(d) Introduce the force derived from the rachet potential $f = -\partial V/\partial x$ and the mobility $\mu$, we find $v_R = v + \mu f$ and an equivalent expression for $v_L = v - \mu f$. Rewrite the Eq. (24) in terms of $v$, $\mu$, and $f$

$$\frac{\partial J}{\partial t} + \alpha J = -J\mu\frac{\partial f}{\partial x} - 2\mu f\frac{\partial J}{\partial x} + 2\mu^2 f P\frac{\partial f}{\partial x} - (v^2 - \mu^2 f^2)\frac{\partial P}{\partial x} + \alpha\mu f P \tag{12}$$

Now use that $J$ is constant in time and regroup the terms to obtain the following expression for the flux

$$J = \frac{1}{1 + \frac{\mu}{\alpha}\frac{\partial f}{\partial x}}\left(\mu f P - \frac{1}{\alpha}\frac{\partial}{\partial x}\left[\left(v^2 - \mu^2 f^2\right)P\right]\right). \tag{13}$$

For the interaction potential, we consider a piecewise form

$$V(x) = \begin{cases} \dfrac{\Delta}{\lambda_1}(\lambda_1 - x) & 0 < x < \lambda_1 \\ \\ \dfrac{\Delta}{\lambda_2}(x - \lambda_1) & \lambda_1 < x < \lambda \end{cases}, \tag{14}$$

where $\lambda = \lambda_1 + \lambda_2$ is the spatial period: $V(x + \lambda) = V(x)$. The barrier height is given by $\Delta$ and we denote by $\delta = \lambda_2 - \lambda_1 \geq 0$ the asymmetry parameter.

(e) Sketch the potential for $\delta = \lambda$, $\delta = \lambda/2$, and $\delta = 0$.

(f) Write down the probability expression for $J$ in the two regions $0 < x < \lambda_1$ (call $P$ in this region $P_1$, analogously $J \to J_1$) and $\lambda_1 < x < \lambda$ ($P \to P_2$ and $J \to J_2$). You will find a set of differential equations for $P_i$ ($i \in \{1, 2\}$).

These can be solved for using the normalization of the probability and flux continuity, which leads to the expression

$$J = \frac{\mu\Delta}{\lambda^2} \frac{\sinh A}{\dfrac{2v^2}{\alpha\mu\Delta} \sinh B \sinh C - \dfrac{\delta}{\lambda} \sinh A}, \tag{15}$$

where $\delta < \delta_c = \lambda - 2\mu\Delta/v$ must hold to ensure that there is a finite flux. That is, particles are not trapped by the potential. The constants $A$, $B$, and $C$ are given by

$$A = \frac{8\delta\alpha\mu^3\Delta^3\lambda^{-3}v^{-4}}{\left[1 + (\delta/\lambda)^2 - (2\mu\Delta/(v\lambda))^2\right]^2 - (2\delta/\lambda)^2}; \tag{16}$$

$$B = \frac{\alpha\mu\Delta}{2v^2} \frac{(1 - \delta/\lambda)^2}{(1 - \delta/\lambda)^2 - (2\mu\Delta/(v\lambda))^2}; \tag{17}$$

$$C = \frac{\alpha\mu\Delta}{2v^2} \frac{(1 + \delta/\lambda)^2}{(1 + \delta/\lambda)^2 - (2\mu\Delta/(v\lambda))^2}. \tag{18}$$

Do not bother to do that yourself!

(g) Give a physical interpretation to the (horrendous mess that is the) above expression. Focus on the relation between flux and potential shape!

(h) Can you come up with a practical way to utilize the ratchet effect on our scale?

## III. MOTILITY INDUCED PHASE SEPARATION

In the last section, we have seen that boundaries can be used to create directed motion in an active system, which is a feature that is not present in classical equilibrium systems, when there is no intrinsic bias. Here, we consider another effect of being out of equilibrium. Figure 4a illustrates the concept of *Motility Induced Phase Separation* (MIPS). It shows a large system comprising active (repulsive) disks, moving at constant velocity $v_0$ and subjected to random reorientation (Brownian rotational diffusion). The core concept behind MIPS is that active particles can come together in such a way that they block each other's progress. This conflict is only resolved once particles

diffuse sufficiently far away from their 'impact' orientation to break the jammed configuration. However, if in the time that it takes to achieve this, more particles come in, which also jam, then the dense phase grows. This growth continues until a steady-state emerges with the — by now substantially reduced in density — remaining (dilute) phase and the condensed active particles exchanging particles on the boundary at constant rate in both directions.

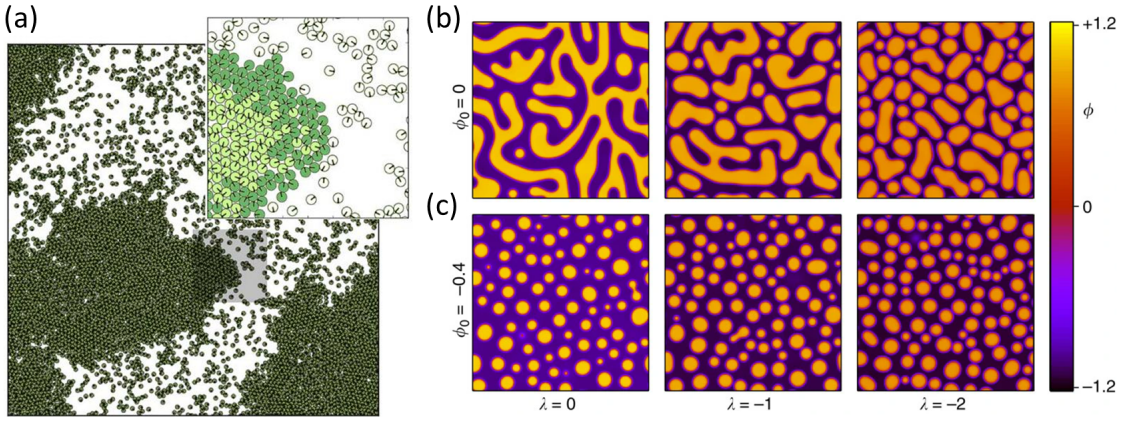


FIG. 4. **Motility Induced Phase Separation:** (a) Purely repulsive active particles with fixed propulsive speed and direction of motion randomized by rotational noise spontaneously phase separate into a dilute gas and a dense phase. This phenomenon is a sort of traffic jam that arises when self-propelled particles slow down due to crowding. It has relevance to bacterial aggregation and assembly of active colloids. (b,c) Sets of snapshots showing the evolving phase separation in two dimensions at fixed time, for increasing levels of non-equilibrium activity $\lambda$ ($\lambda = 0$ is passive). The situation in (b) has a symmetric initial composition ($\varphi_0 = 0$), which gives spinodal-like pattern formation. In (c) the quench is into the region of the phase diagram where the initial composition is asymmetric ($\varphi_0 = -0.4$), which leads to droplet formation. The left figure and caption is taken from the Marchetti group website, while the right figure and caption is adapted from Ref. [62].

MIPS can occur already for volume fractions $\varphi$ as low as 0.3 in numerical simulations [63], at sufficiently high Péclet numbers (Pe $\approx 100$). Here, Pe is a dimensionless number that measures the relative contribution of activity to that of random motion. There are quite a few ways in which this ratio can be defined, but here we choose $\mathrm{Pe} = 3v_0/(2D_r a)$, where $a$ is the particle radius, $v_0$ the active velocity, and $D_r$ the rotational diffusion coefficient (as before). The factor 3 comes from the fact that $D_r = 3D_t/(4a)^2$, where $D_t$ is the translational diffusion coefficient, as before, and is honestly slightly arbitrary, but common in the literature. The physics of this number is captured by the fact that $\tau_r = 1/D_r$ and $v_0\tau_r = l_p$, with $l_p$ the persistence length for the swimmer. This length is compared to the size of the swimmer, $2a$ in this case, and gives an idea how many body lengths the swimmer travels on average before it loses knowledge of its original orientation. To close this point, note that $\varphi = 0.1$ does not give phase separation in equilibrium without attractions.

**Exercise 3:** In this exercise, we will have a first look at MIPS from the perspective of a kinetic argument in 2D, which can be readily generalized to 3D. The active particles in the system have velocity $v_0$, associated Péclet number Pe as defined in the main text, and diameter $\sigma$. We start by assuming a dense phase with a density $\rho_\ell = 2/(\sqrt{3}\sigma^2)$ surrounded by an active gas of (Pe-dependent) density $\rho_g$. We furthermore assume that the area of the dense cluster is large enough to yield an effectively flat vapor-liquid interface.

(a) Explain the factor of $2/\sqrt{3}$ in $\rho_\ell$ and identify the underlying assumption(s). How is this different from equilibrium phase separation?

The incoming flux of particles per unit length from the gas to the liquid is written as $k_{\text{in}}$. The outgoing flux is written $k_{\text{out}}$ and we introduce the notation $\hat{\boldsymbol{n}}$ for an active particle's direction of motion (unit normal) and $\hat{\boldsymbol{s}}$ as the unit normal to the surface of the dense phase.

(b) Argue why $k_{\text{in}} \propto \rho_g v_0$.

(c) Provide an escape criterion using $\hat{\boldsymbol{n}}$ and $\hat{\boldsymbol{s}}$.

(d) Assume that $\hat{\boldsymbol{n}}$ evolves through diffusion and argue that it follows that $k_{\text{out}} \propto D_r/\sigma$. Why should $k_{\text{out}}$ be independent of $v_0$?

(e) Use the steady-state criterion $k_{\text{in}} = k_{\text{out}}$ to solve for $\rho_g$ assuming equalities instead of proportionalities in the respective expressions for the flux. Rewrite this expression in terms of the Péclet number, Pe, as defined in the main text.

In general, the expression in (e) is multiplied by a factor of $q \geq 1$ that accounts for the fact that, when one particle escapes the cluster, it will lead to the escape of additional subsurface particles that had previously been trapped by it. We have $\rho_g = 3\pi q/(\text{Pe}\sigma^2)$.

(f) Using the expressions for $\rho_g$ and $\rho_\ell$, calculate the fraction $\varphi_c$ of particles in the cluster phase, which is defined as

$$\varphi_c \equiv \frac{\rho_\ell V_\ell}{\rho_\ell V_\ell + \rho_g V_g}, \tag{19}$$

where $V_\ell$ and $V_g$ are the respective volumes of the two phases, and show that it reads

$$\varphi_c(\text{Pe}, \rho) = \frac{2\sigma^2\rho\text{Pe} - 6\pi q}{\sigma^2\rho(2\text{Pe} - 3\sqrt{3}\pi q)}. \tag{20}$$

(g) Under what condition can MIPS occur according to (f)? Hint: one of the criteria you get from the above expression obviously needs to be satisfied.

(h) Compute for a system (temperature $T = 300$ K) of active spheres of 1 $\mu$m diameter with an active speed of 1 $\mu\text{ms}^{-1}$ in water (dynamic viscosity $\eta = 10^{-3}$ Pas), the minimum density $\rho$ for MIPS to occur, assuming that $q = 2$.

The kinetic picture sketched above indeed describes the gas binodal at moderate densities.

## IV. THE VICSEK MODEL

Now that we have seen phase separation in an active system, let us turn to some of the other features that collections of active particles can exhibit. The behavior of flocks of birds involve clustering, but these clusters are more dynamic. The *Vicsek model* was developed by Vicsek *et al.* [39] to capture such features. The authors hybridized elements of classical equilibrium models with non-equilibrium features that make the system active. In many regards, the Vicsek model has more the flavor of an algorithm than a theory, as we will see shortly, and it has been studied computationally by many researchers. Unlike MIPS, the dynamics of the Vicsek model are more reminiscent of flow and a hydrodynamic theory can be obtained that matches the large-scale patterns emerging from the microscopic dynamics [42, 64]. Such a theory, however, falls outside the scope of these notes and will be covered in the second part of the *Non-Equilibrium Physics* course.

The Vicsek model is defined by the *overdamped* dynamics of a collection of self-propelled particles (originally) in 2D at density $\rho_0$. For the purpose of an algorithm, this will typically be a square simulation volume with periodic boundary conditions and edge length $L$. The particles are at positions $\boldsymbol{r}_i(t)$ moving along the direction specified by the unit vector $\hat{\boldsymbol{n}}_i(t)$. Here, $i$ is the index and $t$ denotes the time. All particles move with the same constant speed $v_0$, according to the time-discrete (step size $\Delta t$) dynamics

$$\boldsymbol{r}_i(t+\Delta t) = \boldsymbol{r}_i(t) + v_0 \Delta t \hat{\boldsymbol{n}}_i(t), \tag{21}$$

so that orientation and particle velocity have the same direction. Note that the above expression is similar in spirit to the other active matter models we have encountered thus far.

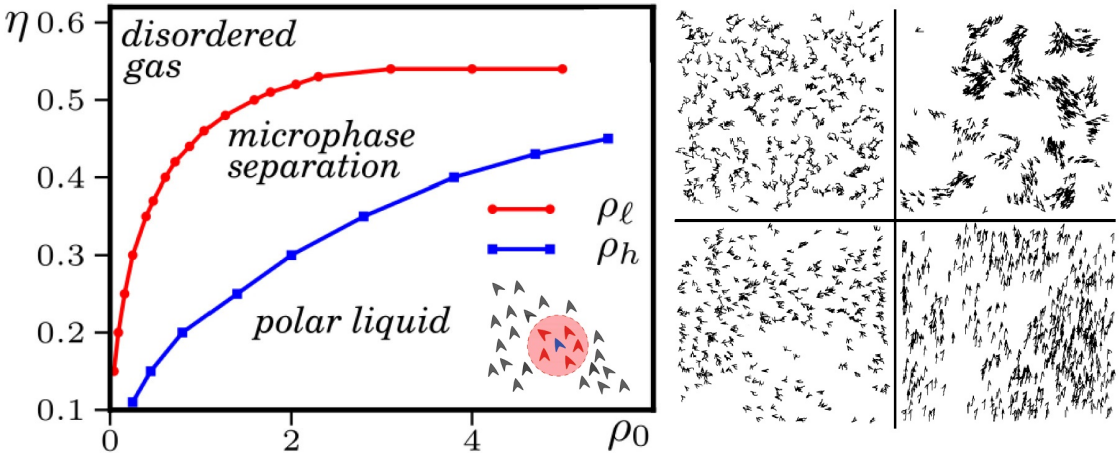


FIG. 5. **The Vicsek Model:** (left panel) The phase diagram for the Vicsek model — density $\rho_0$ and the strength of the noise interfering with alignment $\eta$ are on the respective axes — identifying the three major phases and the parameters for which the transitions occur, taken from Ref. [67]. The colored curves indicate the binodals to the phase separating region. The bottom-right inset visualizes the alignment rule, which was taken from Ref. [68]. (right panel) Snapshots of various phases from the original paper by Vicsek *et al.* [39], showing $N = 300$ self-propelled particles using small wedges. (top-left) Initial condition given by the isotropic phase. (top-right) Low-density and low-noise lead to flocking or equivalently a microphase-separated system. (bottom-left) High-density and high-noise lead to a disordered phase. (bottom-right) High-density and low-noise lead to a polar liquid.

Recall that the ferromagnetic variant of the Ising model has the property that alignment lowers the local energy. Borrowing from the Ising model, Vicsek made the analogy that the direction of motion of a particle is modified by the direction of its neighbors. Because the model is off lattice, this interaction has a range $R_0$, see Fig. 5 for an illustration. In 2D, we can capture the $i$-th particle's orientation using an angle $\theta_i(t)$ (recall the ABP argument), leading to the following angular dynamics

$$\theta_i(t+\Delta t) = \langle \theta_j(t) \rangle_{|\boldsymbol{r}_j(t)-\boldsymbol{r}_i(t)|<R_0} + \Delta\theta, \tag{22}$$

where $\Delta\theta$ is chosen with uniform probability from the interval $[-\eta/2, \eta/2]$. The alignment of a given particle becomes the average — indicated here using the angular brackets and subscript — of all particles in the interaction range. One could think of birds in a flock coordinating with their neighbors, but making small mistakes in doing so.

The parameters defining the Vicsek model are $\rho_0$, $v_0$, $R_0$, and $\eta$. However, $v_0$ can be used to set a time scale in combination with $R_0$, leaving only $\rho_0$ and $\eta$ to control the phase behavior,

for a given $v_0$-$R_0$ combination. The phase behavior is illustrated in Fig. 5. Note specifically that the microphase separated system exhibits a dynamical behavior that is reminiscent of flocking in biological systems. The simple nature of the Vicsek model and its ability to have qualitative similarities to intricate dynamics in biology prompted considerable attention. This has led to an overall shift of the activities of the physics community toward the open problems that are present in biological and even social systems.

Considerable time and effort has been spent figuring out the order of the phase transition in the Vicsek model, which turns out to be quite sensitive to finite-size effects in numerical calculations. Grégoire and Chaté eventually determined that the transition is *first* order [65, 66]. Lastly, it is worth noting that many (often subtle) variants have been proposed and considered.

**Exercise 4:** Implement the Vicsek model and study its phase behavior numerically. If you do not want to bother implementing it, have a look at `https://francescoturci.net/2020/06/19/minimal-vicsek-model-in-python/` instead for a very good `Python` example by Francesco Turci.

## V. ACTIVE FIELD THEORY FOR PHASE-SEPARATION

After our brief excursion into flocking, let us return to the phase behavior of active particles and MIPS. The group led by Mike Cates (University of Cambridge) has been a driving force for theory development in this direction. Here, we briefly give an impression of some of the work to connect to the Cahn-Hilliard description covered in a previous lecture. Let us assume a conserved scalar order-parameter field $\phi(\boldsymbol{r}, t)$ at position $\boldsymbol{r}$ and time $t$. Then we can write an active variant of the Cahn-Hilliard model as

$$\dot{\phi} = -\boldsymbol{\nabla} \cdot \boldsymbol{J}; \tag{23}$$

$$\boldsymbol{J} = -\boldsymbol{\nabla}\mu; \tag{24}$$

$$\mu = -\phi + \phi^3 - \nabla^2\phi + \lambda|\boldsymbol{\nabla}\phi|^2. \tag{25}$$

Here, Eq. (23) expresses conservation of $\phi$ and the dot denotes the time derivative on the left-hand side, while it indicates the inner product on the right; $\boldsymbol{\nabla}$ denotes the gradient operator. Equation (24) states that the mean current $\boldsymbol{J}$ is proportional to the gradient of a nonequilibrium chemical potential $\mu$ obeying Eq. (25). In this last equation, you will find the standard Cahn-Hilliard terms $\phi^3 - \phi$ that follow from a $\phi^4$ local-density approximated free energy and the term $-\nabla^2\phi$ which accounts for the interfacial tension. The passive prefactors have been used to arrive at dimensionfree variables. The unfamiliar term with prefactor $\lambda$ is the key to having an active system. It is the simplest addition to $\mu$, in terms of second-order gradients, that *cannot* be derived from a free-energy functional. N.B. Do not confuse its appearance in $\mu$ with a term of a similar form in $\mathcal{F}$, where it would account for interfacial tension!

The authors of Ref. [62] proposed the model and analyzed it in detail, see also Fig. 4(b,c) for a set of snapshots. They go on to propose an 'uncommon' tangent construction to obtain phase coexistence in this model. This is a major step in reconciling many of the observations that MIPS shared features with equilibrium phase separation:

1. The dense and dilute density stay constant when changing the average density in the coexistence region, given a fixed Pe. In making such a change, the relative volumes occupied by the respective phases satisfy the lever rule.

2. The phase diagram for active (hard) Brownian particles has both binodal and spinodal features, demarking zones of metastability with associated nucleation-and-growth dynamics, and instantaneous decomposition, respectively.

3. The phase-separation kinetics satisfy $L(t) \propto t^{1/3}$, where $L$ is the typical domain size. In equilibrium, this scaling is expected for the process of Oswald ripening: large droplets grow at the expense of small ones through diffusion. You will have unwittingly observed this process in the numerical exercise associated with the Cahn-Hilliard model.

4. The patterns that follow after a quench into the spinodal region are self-similar, in the sense that the structure factor $S(q)$ rescaled by $L(t)$ is stationary.

It should also indicate to you that there may be more similarities between active systems and passive systems than the example of the ratchet suggested.

**Exercise 5:** Read through the sections on the *uncommon-tangent* construction of Ref. [62]. Do you understand the concept and difference to the common-tangent construction? Why do you have to be careful in considering $\phi$?

It should be noted here, that more recent simulation work does not necessarily support the difference in pressure between the two phases. How to develop a theoretical framework for active matter is still an open question. In addition, it is not clear what model captures the essential physics of becoming active in the cleanest manner. Think the equivalent of the Ising model, which is not particularly predictive for any one physical system, but simple enough to be tractable in many situations, while capturing the salient features of many systems.

**Exercise 6:** We will now consider an active variant of the Swift-Hohenberg (SH) model to demonstrate that activity can take other forms in a field-theoretical format. A particular (reduced) real-valued SH equation reads

$$\partial_t u = ru - \left(1 + \nabla^2\right)^2 u - u^3, \tag{26}$$

where $u(\boldsymbol{x}, t)$ is the field, $t$ is the time, $\boldsymbol{x}$ is the position, and $r$ is a control parameter. This is a minimal continuum model for pattern formation near a finite-wavelength instability. In two spatial dimensions (2D) it describes the emergence of stripe (roll) patterns and the formation of defects, which can be understood as topological singularities of an underlying phase field $u$.

(a) Give $u(\boldsymbol{x})$ in the homogeneous, stationary phase. From the shape of the SH equation explain using a *few* words what the physical meaning of the three terms is. Also argue whether the provided SH equation is conservative or not (no calculation is needed).

(b) Linearize the equation and write the resulting PDE explicitly. Insert a plane-wave ansatz $u = \tilde{u}e^{\omega t + i\cdot\boldsymbol{x}}$ with $\tilde{u}$ the amplitude, $i = \sqrt{-1}$, $\omega$ the angular velocity and $k$ the wave vector, and show that the growth rate takes the form $\omega(k) = r - (1 - k^2)^2$. Argue for what value of $r$ a stripe pattern appears (call this $r_c$).

(c) Sketch $\omega(k)$ as a function of $k$ at, below, and above the onset of wave formation; remember to label your curves and axes. What is the critical wave number $k_c$?

Let $r = r_c + \varepsilon$, with $0 < \varepsilon \ll 1$. That is, we are working close to the onset of a wave pattern.

(d) Introduce slow spatial $\boldsymbol{x}$ and temporal $T$ variables appropriate for describing long-wavelength modulations of the pattern. Explain physically why such scales are needed and motivate the ansatz $u(\boldsymbol{x}, t) \approx A(\boldsymbol{x}, T)e^{ik_c\cdot\boldsymbol{x}} + A^*(\boldsymbol{x}, T)e^{-ik_c\cdot\boldsymbol{x}}$, where $A$ is a complex function, the $*$ denotes complex conjugation. What does $A$ encode? Use only *few* words.

Using symmetry arguments it can be shown that the leading-order amplitude dynamics must have the form $\partial_T A = \varepsilon A + \xi \nabla_X^2 A - g|A|^2 A$, with real coefficients $\xi, g > 0$.

(e) Find the uniform steady solution for $|A|$ and relate it to $\varepsilon$. What do you conclude from the scaling about the nature of the phase transition using only a *few* words.

(f) Write $A = \rho e^{i\phi}$ and express the physical stripe pattern in terms of $\rho$ and $\phi$ using part (d). Explain using a *few* words what spatial variations of $\phi$ correspond to physically. Far from defects, $\rho$ can be treated as approximately constant. Explain physically using the equation and a *few* words why the amplitude $\rho$ must vanish at the core of a defect.

(g) Consider a single isolated defect centered at the origin. Assume that far from the core the phase takes the form $\phi(\boldsymbol{x}) = m\theta$, where $\theta$ is the polar angle. Show explicitly that the phase changes by $2\pi m$ upon encircling the defect once using $\oint_\Gamma \mathrm{d}\boldsymbol{x} \cdot \boldsymbol{\nabla}\phi$ with $\Gamma$ the closed path. Explain why $m$ must be an integer using only a *few* words.

Consider a modified SH equation: $\partial_t u = ru - (1+\nabla^2)^2 u - u^3 + \lambda \nabla \cdot \left[(\nabla u)^2 \nabla u\right]$, where $\lambda < 0$ represents activity.

(h) Consider a free-energy density term of the form $f(u) = (\lambda/4)\,(\boldsymbol{\nabla} u)^4$. Write down the free-energy functional $\mathcal{F}$ and compute the contribution of this term to the dynamics of $u$ assuming this dynamics is non-conservative. Why is the modified SH referred to as active, despite the functional form appearing to derive from a functional? Explain using only a *few* words referencing the sign of $\lambda$ and the order of the term.

(i) Argue that near the defect core $\nabla\rho$ is nonzero, while $\rho$ tends to zero, see part (f). Write $\rho(R(t), t) = 0$ as the condition to localize the defect at $\boldsymbol{x} = R(t)$ and provide the time evolution of the $\rho$ field about this defect core. Using a *few* words and a simple calculation, give the conditions for the defect to move persistently and discuss the need for activity.

## VI. SYMMETRY CONSTRAINTS ON THE AMPLITUDE EQUATION

In Exercise 6, we considered a stripe-phase forming theory and active defects therein. One of the elements that was given is the *amplitude equation*. This section is dedicated to understanding how it comes about. The dynamics close to the onset of an instability in many pattern-forming systems can be captured using an amplitude equation. This is because, in such situations, the amplitude of the emerging pattern is small and varies only slowly in space and time. The implied separation of scales allows us to introduce an *amplitude field* that describes the envelope of the pattern, which is reminiscent of how wave packets are analysed. Remarkably, the form of the evolution equation for this amplitude can often be deduced without performing a full perturbative calculation. Instead, the allowed terms follow from the symmetries of the original dynamical equation. This approach is powerful because it reveals that many seemingly different systems share the same large-scale description near the onset of pattern formation.

To illustrate the idea, consider the Swift-Hohenberg equation introduced in the Exercise 6. Linear stability analysis shows that the first unstable mode occurs at a finite wave number $k_c$. Close to the instability the field can therefore be expressed as a modulated periodic pattern

$$u(\boldsymbol{x}, t) \approx A(\boldsymbol{X}, T) e^{i\boldsymbol{k}_c \cdot \boldsymbol{x}} + A^*(\boldsymbol{X}, T) e^{-i\boldsymbol{k}_c \cdot \boldsymbol{x}}, \tag{27}$$

where $A(\boldsymbol{X}, T)$ is the complex amplitude. The slow variables $\boldsymbol{X}$ and $T$ represent spatial and temporal scales that are large compared to the pattern wavelength and oscillation period, respectively. Physically, the complex amplitude $A$ contains two pieces of information. Its magnitude describes the strength of the pattern, while its phase encodes local shifts of the stripes relative to the reference pattern $e^{i\boldsymbol{k}_c\cdot\boldsymbol{x}}$.

Because we are interested in behavior close to the onset of the instability, the control parameter can be written as $r = r_c + \varepsilon$ with $0 < \varepsilon \ll 1$. In this regime the amplitude must remain small, implying that the evolution equation for $A$ can be expanded in powers of $A$ and its spatial derivatives. The key observation is that not all terms are allowed. The structure of the amplitude equation is constrained by the symmetries of the original partial differential equation.

The first important symmetry is *translational invariance*. The Swift-Hohenberg equation is unchanged if all spatial coordinates are shifted by a constant vector $\boldsymbol{a}$. Under such a translation the oscillatory factor in the ansatz transforms as

$$e^{i\boldsymbol{k}_c\cdot\boldsymbol{x}} \to e^{i\boldsymbol{k}_c\cdot(\boldsymbol{x}+\boldsymbol{a})} = e^{i\boldsymbol{k}_c\cdot\boldsymbol{a}} e^{i\boldsymbol{k}_c\cdot\boldsymbol{x}}. \tag{28}$$

In order for the field $u(\boldsymbol{x}, t)$ to remain unchanged, the amplitude must transform according to $A \to Ae^{i\theta}$, where $\theta = \boldsymbol{k}_c \cdot \boldsymbol{a}$ is a constant phase. Consequently, the amplitude equation must be invariant under a global phase transformation of $A$. This requirement strongly restricts the possible nonlinear terms.

**Exercise 7:** Consider the amplitude representation introduced in the text,

$$u(\boldsymbol{x}, t) \approx A(\boldsymbol{X}, T)e^{i\boldsymbol{k}_c\cdot\boldsymbol{x}} + A^*(\boldsymbol{X}, T)e^{-i\boldsymbol{k}_c\cdot\boldsymbol{x}}, \tag{29}$$

where $A$ is a complex amplitude that varies slowly in space and time. Recall that the original equation is invariant under spatial translations $\boldsymbol{x} \to \boldsymbol{x} + \boldsymbol{a}$. Under such a transformation the phase factor changes as

$$e^{i\boldsymbol{k}_c\cdot\boldsymbol{x}} \to e^{i\boldsymbol{k}_c\cdot\boldsymbol{a}} e^{i\boldsymbol{k}_c\cdot\boldsymbol{x}}, \tag{30}$$

which implies that the amplitude transforms as $A \to Ae^{i\theta}$, where $\theta = \boldsymbol{k}_c \cdot \boldsymbol{a}$ is a constant phase.

(a) Using this transformation rule, show explicitly how the expressions $A$, $|A|^2A$, $A^2$, and $A^*$ transform under the phase shift $A \to Ae^{i\theta}$.

(b) Determine which of these expressions remain invariant under the phase transformation.

(c) Using only a *few* words, explain why the non-invariant expressions cannot appear in the amplitude equation for $A$ if the underlying physical system is translationally invariant.

A second constraint follows from the isotropy of space. The Swift-Hohenberg equation does not single out any preferred spatial direction. The amplitude equation must therefore also respect rotational symmetry. The lowest-order spatial operator compatible with isotropy is the Laplacian $\nabla^2 A$. Terms involving a single derivative, such as $\partial_X A$, would introduce a preferred direction and are therefore not allowed. As a result, spatial modulations of the amplitude enter the dynamics through diffusive-like terms involving $\nabla^2 A$.

**Exercise 8:** Consider again the complex amplitude $A(\boldsymbol{X}, T)$ describing slow modulations of the stripe pattern. The original Swift-Hohenberg equation is isotropic in space, meaning that it is invariant under rotations of the coordinate system. Consequently, the amplitude equation must also respect rotational symmetry.

(a) Consider the following candidate spatial terms that could appear in the amplitude dynamics $\partial_X A$, $\partial_X^2 A$, $\partial_X \partial_Y A$, and $\nabla^2 A$. Explain using a *few* words which of these terms introduce a preferred spatial direction and are therefore incompatible with rotational symmetry.

(b) Show explicitly that the Laplacian

$$\nabla^2 A = \partial_X^2 A + \partial_Y^2 A \tag{31}$$

remains unchanged under a rotation of the coordinate system. Hint: you may argue geometrically or by recalling a known property of the Laplacian.

(c) Higher-order spatial derivatives may also appear in principle. Give two examples of higher-order isotropic operators acting on $A$ that are consistent with rotational symmetry.

(d) Explain using a *few* words why such higher-order operators are typically neglected in the leading-order amplitude equation close to the instability threshold.

A third constraint arises from the fact that the physical field $u(\boldsymbol{x}, t)$ is real. The amplitude representation includes both $A$ and its complex conjugate $A^*$ in order to satisfy this requirement. Consistency of the dynamics under complex conjugation implies that the coefficients appearing in the amplitude equation must be real at leading order.

Finally, nonlinear effects must eventually halt the exponential growth of the instability above threshold. The lowest-order nonlinear term compatible with the phase symmetry is proportional to $|A|^2 A$. Higher-order contributions such as $|A|^4 A$ are also possible in principle but are smaller close to onset and can therefore be neglected at leading order. Collecting all allowed contributions then leads to the amplitude equation

$$\partial_T A = \varepsilon A + \xi \nabla_X^2 A - g|A|^2 A, \tag{32}$$

where $\xi$ and $g$ are real coefficients whose precise values depend on the details of the underlying equation. For the Swift–Hohenberg model one finds $g > 0$, ensuring that the instability saturates at a finite amplitude. This equation is often referred to as the *real Ginzburg-Landau amplitude equation*. It appears in a wide variety of pattern-forming systems and therefore represents a universal description of stripe patterns near their onset.

### A. A Practical Recipe for Constructing Amplitude Equations

When encountering a pattern-forming instability, it is often useful to follow a systematic procedure to determine the form of the amplitude dynamics. The first step is to identify the critical mode from the linear stability analysis and write the physical field as a slowly modulated periodic pattern whose envelope is described by a complex amplitude $A(\boldsymbol{X}, T)$. The slow variables $\boldsymbol{X}$ and $T$ represent the long spatial and temporal scales over which the envelope changes.

The second step is to list the symmetries of the original equation. Typical examples include spatial translation invariance, rotational symmetry, and the requirement that the physical field be real. These symmetries determine how the amplitude transforms. In the present case translational invariance implies that $A$ can acquire an arbitrary global phase without changing the physical field.

The third step is to write down the most general evolution equation for $A$ that is consistent with these symmetries. One includes all possible combinations of $A$ and its spatial derivatives that remain invariant under the symmetry transformations. At this stage the coefficients multiplying each term remain undetermined.

The final step is to organize the resulting expression in powers of the amplitude and its gradients. Close to the instability threshold both the amplitude and its spatial variations are small. One therefore keeps only the lowest-order contributions in this expansion. The resulting equation describes the leading-order dynamics of the pattern envelope and is often universal, meaning that many different microscopic models reduce to the same amplitude equation near onset.

### B. Amplitude-Phase Representation of the Pattern

It is often convenient to write the complex amplitude in polar form,

$$A(\boldsymbol{X}, T) = \rho(\boldsymbol{X}, T)\, e^{i\phi(\boldsymbol{X},T)}, \tag{33}$$

where $\rho \geq 0$ is the amplitude (or magnitude) and $\phi$ is the phase. Inserting this representation into the expression for the physical field gives

$$u(\boldsymbol{x}, t) \approx \rho(\boldsymbol{X}, T) e^{i(\boldsymbol{k}_c \cdot \boldsymbol{x} + \phi)} + \rho(\boldsymbol{X}, T) e^{-i(\boldsymbol{k}_c \cdot \boldsymbol{x} + \phi)}. \tag{34}$$

Using the identity $e^{i\theta} + e^{-i\theta} = 2\cos\theta$, the stripe pattern can be written as

$$u(\boldsymbol{x}, t) \approx 2\rho(\boldsymbol{X}, T) \cos\big(\boldsymbol{k}_c \cdot \boldsymbol{x} + \phi(\boldsymbol{X}, T)\big)\,. \tag{35}$$

This expression clearly separates two physical ingredients of the pattern. The amplitude $\rho$ determines the strength of the modulation, *i.e.*, how pronounced the stripes are, while the phase $\phi$ describes spatial shifts of the pattern. A spatial variation of $\phi$ corresponds to a local displacement of the stripes. In other words, the phase field acts as a slowly varying coordinate that tracks how the periodic pattern is distorted across space.

Far away from singular structures, the amplitude varies only weakly, so that the dominant degrees of freedom are often encoded in the phase field. However, there may be *topological defects* in the stripe patter, where the where the phase becomes singular. To understand why the amplitude $\rho$ must vanish at the center of a defect, it is useful to consider the structure of the phase field around such a point. A common form for the phase far from an isolated defect located at the origin is

$$\phi(\boldsymbol{x}) = m\theta, \tag{36}$$

where $\theta$ is the polar angle and $m$ is an integer known as the *topological charge*. When moving once around the defect, the polar angle changes by $2\pi$, and therefore the phase changes by $2\pi m$. The pattern thus winds around the defect. We have seen this in the context of the continuous form of the $XY$ model previously, here we consider this for more complex free-energy forms. The key observation is that the phase $\phi$ cannot be defined continuously at the origin. The angular coordinate $\theta$ is undefined there, meaning that the phase field becomes singular at the defect core. If the amplitude $\rho$ remained finite at that point, the complex amplitude

$$A = \rho e^{i\phi} \tag{37}$$

would also be ill-defined because the phase would be ambiguous. That is, it can assume a range of values, depending on the $\phi$-direction from which the origin is approached.

The system avoids this problem by allowing the magnitude $\rho$ to go to zero at the defect core. When $\rho = 0$, the value of the phase becomes irrelevant because

$$A = 0 \tag{38}$$

independently of $\phi$. In physical terms, this means that the stripe pattern disappears locally at the defect center, removing the singularity of the phase field. The vanishing amplitude therefore regularizes the field and ensures that the physical solution remains well-defined everywhere. Another way to view this result is through energetic considerations. Spatial variations of the phase contribute gradient terms such as $|\nabla\phi|^2$ to the effective description of the amplitude dynamics. Near a defect core the phase varies rapidly, which would lead to a large energetic cost if the amplitude remained finite. Allowing $\rho$ to decrease locally reduces this cost, and the minimum-energy configuration therefore corresponds to $\rho \to 0$ at the defect center.

In summary, a topological defect corresponds to a singular configuration of the phase field, and the amplitude must vanish at the core to keep the complex field $A$ and the physical field $u$ well defined. This behavior is generic in systems described by complex order parameters and appears in many areas of physics, including superfluids, superconductors, and pattern-forming systems.

**Exercise 9:** In the previous exercises, we considered stripe patterns described by a single complex amplitude. Many pattern-forming systems, however, exhibit more complex structures. One important example is the *hexagonal phase*, which appears in variants of the conserved Swift-Hohenberg equation and in many physical systems such as convection, block copolymers, and crystalline order in soft matter. Close to onset, a hexagonal pattern can be represented as a superposition of three plane waves whose wave vectors form 120° angles with each other,

$$u(\boldsymbol{x},t) \approx \sum_{j=1}^{3} \left[ A_j(\boldsymbol{X},T) e^{i\boldsymbol{k}_j\cdot\boldsymbol{x}} + A_j^*(\boldsymbol{X},T) e^{-i\boldsymbol{k}_j\cdot\boldsymbol{x}} \right], \tag{39}$$

where the three wave vectors satisfy $|\boldsymbol{k}_j| = k_c$ and $\boldsymbol{k}_1 + \boldsymbol{k}_2 + \boldsymbol{k}_3 = 0$. Each complex amplitude can be written as $A_j = \rho_j e^{i\phi_j}$.

(a) Using the identity $e^{i\theta} + e^{-i\theta} = 2\cos\theta$, rewrite the expression for $u(\boldsymbol{x},t)$ in terms of $\rho_j$ and $\phi_j$. Explain using a *few* words what physical information is encoded in the amplitudes $\rho_j$ and the phases $\phi_j$.

(b) Suppose that far from defects all amplitudes take the same constant value $\rho_j = \rho_0$. Show that the resulting pattern corresponds to a hexagonal lattice of peaks in $u(\boldsymbol{x},t)$.

(c) Consider slowly varying phase fields $\phi_j(\boldsymbol{x})$. Explain using a *few* words how spatial gradients of the phases correspond to local distortions or displacements of the hexagonal lattice.

(d) In crystalline solids, one common defect is a *dislocation*. Around such a defect the lattice is shifted by one lattice spacing when moving once around the defect core. Argue qualitatively how such a defect could be represented in terms of the phases $\phi_j$.

(e) As in the stripe case, the phases $\phi_j$ may become singular at the defect core. Explain using a *few* words why at least one of the amplitudes $\rho_j$ must vanish near the core in order for the physical field $u(\boldsymbol{x},t)$ to remain well defined.

(f) Compare the situation with the stripe pattern discussed earlier. Explain using a *few* words why hexagonal patterns can support a richer variety of defects than stripes.

This exercise illustrates how defects in pattern-forming systems are closely related to defects in crystalline materials. In both cases the underlying idea is that slowly varying phase fields describe local displacements of a periodic structure, while singularities in these phase fields correspond to topological defects of the pattern.

## VII. FINAL THOUGHTS

Summarizing, we have discussed various models of active systems, including Active Brownian Particles and the Vicsek model. We have also shown some basic features that distinguish active systems from their passive counterparts. For example, active systems can exhibit currents in steady state, which may be exploited to harvest work from the system. Motility Induced Phase Separation describes a process of geometric frustration balancing diffusion-based escape from clusters, which can force the system to phase separate at much lower densities than available to a passive system. Yet, surprisingly, there are perhaps fewer differences between active and passive systems than these two scenarios suggest. We explored this aspect on the basis of an effective, phase-field description of MIPS that had connections to the Cahn-Hilliard model discussed in a previous lecture. It should be noted, however, that the list of topics we covered in this lecture is by no means exhaustive. We have, for example, ignored active turbulence and active solids.

In terms of the future of the field, a lot of attention is currently being spent on active matter without particle conservation. This includes bacterial colony growth (*e.g.*, see Refs. [69–71] and citations therein), and tissue dynamics in wound healing, cancer spread, and development [72–75]. A more recent focus is *smart* matter [76]. That is, active matter that is not only able to move, but also able to perform basic arithmetic and/or have emergent complex behaviors reminiscent of (collections of) neurons. Another branch of active matter is moving into the direction of behavioral models, *i.e.*, models with vision that can model basic aspects of predator-prey interactions [77]. Lastly, understanding and working with artificial motors has received considerable attention [55, 78, 79]. Much work has been done using agent-based models in these areas, but there is also a lot of room for analytic and computational theory.

[1] A. Archer and R. Evans, *Dynamical density functional theory and its application to spinodal decomposition*, J. Chem. Phys. **121**, 4246 (2004).

[2] M. Ballerini *et al.*, *Interaction ruling animal collective behavior depends on topological rather than metric distance: Evidence from a field study*, Proc. Natl. Acad. Sci. **105**, 1232 (2008).

[3] Y. Katz, K. Tunstrøm, C. Ioannou, C. Huepe, and I. Couzin, *Inferring the structure and dynamics of interactions in schooling fish*, Proc. Nat. Acad. Sci. **108**, 18720 (2011).

[4] D. Helbing, I. Farkas, and T. Vicsek, *Simulating dynamical features of escape panic*, Nature **407**, 487 (2000).

[5] J. Zhang, W. Klingsch, A. Schadschneider, and A. Seyfried, in *Traffic and Granular Flow '11*, edited by V. V. Kozlov, A. P. Buslaev, A. S. Bugaev, M. V. Yashina, A. Schadschneider, and M. Schreckenberg (Springer (Berlin/Heidelberg), ADDRESS, 2013), p. 241.

[6] J. Silverberg, M. Bierbaum, J. Sethna, and I. Cohen, *Collective motion of humans in mosh and circle pits at heavy metal concerts*, Phys. Rev. Lett. **110**, 228701 (2013).

[7] A. Sokolov, I. Aranson, J. Kessler, and R. Goldstein, *Concentration dependence of the collective dynamics of swimming bacteria*, Phys. Rev. Lett. **98**, 158102 (2007).

[8] J. Schwarz-Linek, C. Valeriani, A. Cacciuto, M. E. Cates, D. Marenduzzo, A. N. Morozov, and W. C. K. Poon, *Phase separation and rotor self-assembly in active particle suspensions*, Proc. Nat. Acad. Sci. **109**, 4052 (2012).

[9] M. Reufer, R. Besseling, J. Schwarz-Linek, V. Martinez, A. Morozov, J. Arlt, D. Trubitsyn, F. Ward, and W. Poon, *Switching of swimming modes in magnetospirillium gryphiswaldense*, Biophys. J. **106**, 37 (2014).

[10] D. Woolley, *Motility of spermatozoa at surfaces*, Reproduction **126**, 259 (2003).

[11] I. Riedel, K. Kruse, and J. Howard, *A self-organized vortex array of hydrodynamically entrained sperm cells*, Science **309**, 300 (2005).

[12] R. Ma, G. Klindt, I. Riedel-Kruse, F. Jülicher, and B. Friedrich, *Active phase and amplitude fluctuations of flagellar beating*, Phys. Rev. Lett. **113**, 048101 (2014).

[13] M. Polin, I. Tuval, K. Drescher, J. Gollub, and R. Goldstein, *Chlamydomonas swims with two "gears" in a eukaryotic version of run-and-tumble locomotion*, Science **325**, 487 (2009).

[14] V. Geyer, F. Jülicher, J. Howard, and B. Friedrich, *Cell-body rocking is a dominant mechanism for flagellar synchronization in a swimming alga*, Proc. Nat. Acad. Sci. **110**, 18058 (2013).

[15] D. Mizuno, C. Tardin, C. Schmidt, and F. MacKintosh, *Nonequilibrium mechanics of active cytoskeletal networks*, Science **315**, 370 (2007).

[16] R. Ismagilov, A. Schwartz, N. Bowden, and G. Whitesides, *Autonomous movement and self-assembly*, Angew. Chem. Int. Ed. **41**, 652 (2002).

[17] W. F. Paxton, K. C. Kistler, C. C. Olmeda, A. Sen, S. K. St. Angelo, Y. Cao, T. E. Mallouk, P. E. Lammert, and V. H. Crespi, *Catalytic nanomotors: Autonomous movement of striped nanorods*, J. Am. Chem. Soc. **126**, 13424 (2004).

[18] Y. Wang, R. M. Hernandez, D. J. Bartlett, J. M. Bingham, T. R. Kline, A. Sen, and T. E. Mallouk, *Bipolar electrochemical mechanism for the propulsion of catalytic nanomotors in hydrogen peroxide solutions*, Langmuir **22**, 10451 (2006).

[19] A. Brown and W. Poon, *Ionic effects in self-propelled pt-coated janus swimmers*, Soft Matter **10**, 4016 (2014).

[20] S. Ebbens, D. Gregory, G. Dunderdale, J. Howse, Y. Ibrahim, T. Liverpool, and R. Golestanian, *Electrokinetic effects in catalytic platinum-insulator janus swimmers*, Euro. Phys. Lett. **106**, 58003 (2014).

[21] S. Ebbens, M.-H. Tu, J. R. Howse, and R. Golestanian, *Size dependence of the propulsion velocity for catalytic janus-sphere swimmers*, Phys. Rev. E **85**, 020401 (2012).

[22] J. R. Howse, R. A. L. Jones, A. J. Ryan, T. Gough, R. Vafabakhsh, and R. Golestanian, *Self-motile colloidal particles: From directed propulsion to random walk*, Phys. Rev. Lett. **99**, 048102 (2007).

[23] L. F. Valadares, Y.-G. Tao, N. S. Zacharia, V. Kitaev, F. Galembeck, R. Kapral, and G. A. Ozin, *Catalytic nanomotors: Self-propelled sphere dimers*, Small **6**, 565 (2010).

[24] J. Simmchen, V. Magdanz, S. Sanchez, S. Chokmaviroj, D. Ruiz-Molina, A. Baeza, and O. Schmidt, *Effect of surfactants on the performance of tubular and spherical micromotors – a comparative study*,

RSC Adv. **4**, 20334 (2014).
[25] H.-R. Jiang, N. Yoshinaga, and M. Sano, *Active motion of a janus particle by self-thermophoresis in a defocused laser beam*, Phys. Rev. Lett. **105**, 268302 (2010).
[26] L. Baraban, R. Streubel, D. Makarov, L. Han, D. Karnaushenko, O. G. Schmidt, and G. Cuniberti, *Fuel-free locomotion of janus motors: Magnetically induced thermophoresis*, ACS Nano **7**, 1360 (2013).
[27] I. Buttinoni, G. Volpe, F. Kümmel, G. Volpe, and C. Bechinger, *Active brownian motion tunable by light*, J. Phys.: Condens. Matter **24**, 284129 (2012).
[28] A. A. Solovev, Y. Mei, E. Bermúdez Ureña, G. Huang, and O. G. Schmidt, *Catalytic microtubular jet engines self-propelled by accumulated gas bubbles*, Small **5**, 1688 (2009).
[29] Y. Mei, A. A. Solovev, S. Sanchez, and O. G. Schmidt, *Rolled-up nanotech on polymers: from basic perception to self-propelled catalytic microengines*, Chem. Soc. Rev. **40**, 2109 (2011).
[30] M. Cates, *Diffusive transport without detailed balance in motile bacteria: does microbiology need statistical physics?*, Rep. Prog. Phys. **75**, 042601 (2012).
[31] M. Cates and J. Tailleur, *Motility-induced phase separation*, Annu. Rev. Condens. Matter Phys. **6**, 219 (2015).
[32] T. E. Mallouk and A. Sen, *Powering nanorobots*, Sci. Am. **300**, 72 (2009).
[33] M. Popescu, S. Dietrich, M. Tasinkevych, and J. Ralston, *Phoretic motion of spheroidal particles due to self-generated solute gradients*, Eur. Phys. J. E **31**, 351 (2010).
[34] S. Das, A. Garg, A. Campbell, J. Howse, A. Sen, D. Velegol, R. Golestanian, and S. Ebbens, *Boundaries can steer active janus spheres*, Nat. Commun. **6**, 8999 (2015).
[35] A. Brown, W. Poon, C. Holm, and J. De Graaf, *Ionic screening and dissociation are crucial for understanding chemical self-propulsion in polar solvents*, Soft Matter **13**, 1200 (2017).
[36] J. de Graaf, G. Rempfer, and C. Holm, *Diffusiophoretic self-propulsion for partially catalytic spherical colloids*, IEEE Trans. Nanobiosci. **14**, 272 (2015).
[37] S. Ketzetzi, J. De Graaf, R. Doherty, and D. Kraft, *Slip length dependent propulsion speed of catalytic colloidal swimmers near walls*, Phys. Rev. Lett. **124**, 048002 (2020).
[38] S. Ketzetzi, J. De Graaf, and D. Kraft, *Diffusion-based height analysis reveals robust microswimmer-wall separation*, Phys. Rev. Lett. **125**, 238001 (2020).
[39] T. Vicsek, A. Czirók, E. Ben-Jacob, I. Cohen, and O. Shochet, *Novel type of phase transition in a system of self-driven particles*, Phys. Rev. Lett. **75**, 1226 (1995).
[40] J. Toner and Y. Tu, *Long-range order in a two-dimensional dynamical xy model: how birds fly together*, Phys. Rev. Lett. **75**, 4326 (1995).
[41] J. Toner and Y. Tu, *Flocks, herds, and schools: A quantitative theory of flocking*, Phys. Rev. E **58**, 4828 (1998).
[42] J. Toner, Y. Tu, and S. Ramaswamy, *Hydrodynamics and phases of flocks*, Ann. Phys. **318**, 170 (2005).
[43] T. Sanchez, D. Chen, S. DeCamp, M. Heymann, and Z. Dogic, *Spontaneous motion in hierarchically assembled active matter*, Nature **491**, 431 (2012).
[44] L. Giomi, M. Bowick, X. Ma, and M. Marchetti, *Defect annihilation and proliferation in active nematics*, Phys. Rev. Lett. **110**, 228101 (2013).
[45] L. Giomi, *Geometry and topology of turbulence in active nematics*, Phys. Rev. X **5**, 031003 (2015).
[46] S. DeCamp, G. Redner, A. Baskaran, M. Hagan, and Z. Dogic, *Orientational order of motile defects in active nematics*, Nat. Mater. **14**, 1110 (2015).
[47] L. Lemma, S. DeCamp, Z. You, L. Giomi, and Z. Dogic, *Statistical properties of autonomous flows in 2d active nematics*, Soft Matter **15**, 3264 (2019).
[48] S. Shankar, A. Souslov, M. Bowick, M. Marchetti, and V. Vitelli, *Topological active matter*, Nat. Reb. Phys. **4**, 380 (2022).
[49] M. Bowick, N. Fakhri, M. Marchetti, and S. Ramaswamy, *Symmetry, thermodynamics, and topology in active matter*, Phys. Rev. X **12**, 010501 (2022).
[50] A. Einstein, *Eine neue bestimmung der moleküldimension*, Ann. Phys. **19**, 289 (1906).
[51] G. Volpe, I. Buttinoni, D. Vogt, H.-J. Kummerer, and C. Bechinger, *Microswimmers in patterned environments*, Soft Matter **7**, 8810 (2011).
[52] J. Simmchen, J. Katuri, W. Uspal, M. Popescu, M. Tasinkevych, and S. Sánchez, *Topographical pathways guide chemical microswimmers*, Nat. Commun. **7**, 10598 (2016).
[53] S. Ketzetzi, M. Rinaldin, P. Dröge, J. de Graaf, and D. Kraft, *Activity-induced interactions and cooperation of artificial microswimmers in one-dimensional environments*, Nat. Commun. **13**, 1772 (2022).

[54] É. Fodor and M. Marchetti, *The statistical physics of active matter: From self-catalytic colloids to living cells*, Phys. A: Stat. Mech. **504**, 106 (2018).

[55] C. Bechinger, R. Di Leonardo, H. Löwen, C. Reichhardt, G. Volpe, and G. Volpe, *Active particles in complex and crowded environments*, Rev. Mod. Phys. **88**, 045006 (2016).

[56] L. Turner, W. Ryu, and H. Berg, *Real-time imaging of fluorescent flagellar filaments*, J. Bacteriol. **182**, 2793 (2000).

[57] Y. Zhao *et al.*, *Quantitative characterization of run-and-tumble statistics in bulk bacterial suspensions*, arXiv **2212.10996**, 1 (2022).

[58] L. Angelani, R. Di Leonardo, and G. Ruocco, *Self-starting micromotors in a bacterial bath*, Phys. Rev. Lett. **102**, 048104 (2009).

[59] R. Di Leonardo *et al.*, *Bacterial ratchet motors*, Proc. Nat. Acad. Sci. **107**, 9541 (2010).

[60] P. Ghosh, V. Misko, F. Marchesoni, and F. Nori, *Self-propelled janus particles in a ratchet: Numerical simulations*, Phys. Rev. Lett. **110**, 268301 (2013).

[61] J. Katuri, D. Caballero, R. Voituriez, J. Samitier, and S. Sanchez, *Directed flow of micromotors through alignment interactions with micropatterned ratchets*, ACS Nano **12**, 7282 (2018).

[62] R. Wittkowski, A. Tiribocchi, J. Stenhammar, R. Allen, D. Marenduzzo, and M. Cates, *Scalar $\varphi^4$ field theory for active-particle phase separation*, Nat. Commun. **5**, 4351 (2014).

[63] J. Stenhammar, D. Marenduzzo, R. Allen, and M. Cates, *Phase behaviour of active brownian particles: the role of dimensionality*, Soft Matter **10**, 1489 (2014).

[64] F. Ginelli, *The physics of the vicsek model*, Euro. Phys. J. S.T. **225**, 2099 (2016).

[65] A. Solon, H. Chaté, and J. Tailleur, *From phase to microphase separation in flocking models: The essential role of nonequilibrium fluctuations*, Phys. Rev. Lett. **114**, 068101 (2015).

[66] M. Zumaya, H. Larralde, and M. Aldana, *Delay in the dispersal of flocks moving in unbounded space using long-range interactions*, Sci. Reports **8**, 1 (2018).

[67] G. Grégoire and H. Chaté, *Onset of collective and cohesive motion*, Phys. Rev. Lett. **92**, 025702 (2004).

[68] H. Chaté, F. Ginelli, G. Grégoire, and F. Raynaud, *Collective motion of self-propelled particles interacting without cohesion*, Phys. Rev. E **77**, 046113 (2008).

[69] A. Martínez-Calvo, T. Bhattacharjee, R. Bay, H. Luu, A. Hancock, N. Wingreen, and S. Datta, *Morphological instability and roughening of growing 3d bacterial colonies*, Proc. Nat. Acad. Sci. **119**, e2208019119 (2022).

[70] A. Golden, I. Dukovski, D. Segrè, and K. Korolev, *Growth instabilities shape morphology and genetic diversity of microbial colonies*, Phys. Biol. **19**, 056005 (2022).

[71] P. Bravo, S. Lung Ng, K. MacGillivray, B. Hammer, and P. Yunker, *Vertical growth dynamics of biofilms*, Proc. Nat. Acad. Sci. **120**, e2214211120 (2023).

[72] B. Camley and W.-J. Rappel, *Physical models of collective cell motility: from cell to tissue*, J. Phys. D: Appl. Phys. **50**, 113002 (2017).

[73] D. Barton, S. Henkes, C. Weijer, and R. Sknepnek, *Active vertex model for cell-resolution description of epithelial tissue mechanics*, PLoS Comput. Biol. **13**, e1005569 (2017).

[74] R. Alert and X. Trepat, *Physical models of collective cell migration*, Ann. Rev. Cond. Mat. Phys. **11**, 77 (2020).

[75] J. Metzcar, Y. Wang, R. Heiland, and P. Macklin, *A review of cell-based computational modeling in cancer biology*, JCO Clin. Cancer Inform. **2**, 1 (2019).

[76] H. Levine and D. Goldman, *Physics of smart matter: integrating active matter and control to gain insights into living systems*, arXiv **2302.00234**, 1 (2023).

[77] F. Lavergne, H. Wendehenne, T. Bäuerle, and C. Bechinger, *Group formation and cohesion of active particles with visual perception–dependent motility*, Science **364**, 70 (2019).

[78] W. Wang, W. Duan, S. Ahmed, T. Mallouk, and A. Sen, *Small power: Autonomous nano-and micromotors propelled by self-generated gradients*, Nano Today **8**, 531 (2013).

[79] M. Fernández-Medina, M. Ramos-Docampo, O. Hovorka, V. Salgueiriño, and B. Städler, *Recent advances in nano-and micromotors*, Adv. Funct. Mat. **30**, 1908283 (2020).